$(Mn_zFe_{1-z})_yO_x$ Combined Oxides as Oxygen Carrier for Chemical-Looping with Oxygen Uncoupling

Golnar Azimi
Dept. of Environmental Inorganic Chemistry, Chalmers University of Technology, S-412 96 Göteborg, Sweden

Magnus Rydén
Dept. of Energy and Environment, Chalmers University of Technology, S-412 96 Göteborg, Sweden

Henrik Leion
Dept. of Environmental Inorganic Chemistry, Chalmers University of Technology, S-412 96 Göteborg, Sweden

Tobias Mattisson and Anders Lyngfelt
Dept. of Energy and Environment, Chalmers University of Technology, S-412 96 Göteborg, Sweden

DOI 10.1002/aic.13847
Published online June 7, 2012 in Wiley Online Library (wileyonlinelibrary.com).

Oxygen carrier particles with the composition $(Mn_{0.8},Fe_{0.2})_2O_3$ were found to readily release gas phase oxygen at 850°C, and were capable to oxidize CH_4 completely and convert wood char rapidly to CO_2 during experiments in a batch fluidized bed reactor. The particles were able to release oxygen corresponding to more than 3% of their mass in less than 40 s. Because of the low price and favourable environmental properties of manganese and iron oxides, this finding could be of great importance for the development of chemical-looping combustion with oxygen uncoupling. © 2012 American Institute of Chemical Engineers *AIChE J,* 59: 582–588, 2013
Keywords: CO_2 capture, chemical-looping combustion, chemical-looping with oxygen uncoupling, iron manganese oxide

Introduction: Chemical-Looping Combustion with Oxygen Uncoupling

Chemical-looping combustion (CLC) is an innovative method to oxidize fuel that utilizes two separate reactors, one air reactor and one fuel reactor. A solid oxygen carrier performs the task of transporting oxygen between the two reactors. In the fuel reactor, the oxygen carrier is reduced by the fuel, which in turn is oxidized to CO_2 and H_2O. In the air reactor, the oxygen carrier is reoxidized to its initial state with O_2 from air. The sum of reactions and net energy released are the same as in ordinary combustion, and the concept has several attractive features. Most importantly, the gas from the fuel reactor consists essentially of CO_2 and H_2O. Cooling in a condenser is all that is needed to obtain almost pure CO_2, which makes CLC an ideal technology for heat and power production with carbon sequestration. Progress within this area has been reviewed recently by Lyngfelt et al.,[1,2] Fang et al.,[3] and Hossain et al.[4]

One notable variant of the CLC concept is so-called chemical-looping with oxygen uncoupling (CLOU). Here, an oxygen carrier material which releases gas phase O_2 directly into the fuel reactor is used. The resulting sum of reactions is identical to CLC, but the mechanism for oxidation of the fuel is different. In ordinary CLC, the oxidation takes place mainly via gas-solids reactions. Consequently, if a solid fuel such as coal or biomass is used it has to be gasified to be able to react with the oxygen carrier. By contrast, in CLOU the fuel can react directly with released O_2 and does not need to be gasified. Experiments by Mattisson et al.[5] and Leion et al.[6] show that oxidation of solid fuels such as petroleum coke can be 45 times faster with CLOU, compared to ordinary CLC.

A feasible oxygen-carrier material for CLOU should be thermodynamically capable to take up and release gas-phase O_2 at relevant conditions, provide sufficiently fast reaction kinetics for the O_2 uncoupling and the oxidation reactions, have a decently high content of active oxygen and preferably be cheap and nontoxic. Many commonly proposed oxygen carriers for CLC such as NiO and Fe_2O_3 fail to satisfy the first of these requirements, that is, they cannot release gas phase O_2 at relevant conditions. The most examined oxide pair for CLC with oxygen uncoupling is CuO–Cu_2O, which has been found to work well.[5,6] But, the low melting point of metallic copper could be an obstacle, and CuO is also fairly costly. In theory, the oxide pair Mn_2O_3–Mn_3O_4 could also work, see Mattisson et al.[7] But experiments with unmodified manganese oxides show no or very low O_2 release at relevant conditions. This is likely an effect of the low temperature needed to have a suitable equilibrium concentration of O_2 for Mn_2O_3–Mn_3O_4, that is, slightly below 800°C.

Properties of $(Mn_zFe_{1-z})_yO_x$ Combined Oxides

Several recent studies have shown that it is possible to alter the thermodynamic properties of manganese oxides by combination with other cations. Many such combined oxides

Correspondence concerning this article should be addressed to G. Azimi at golnar.azimi@chalmers.se.

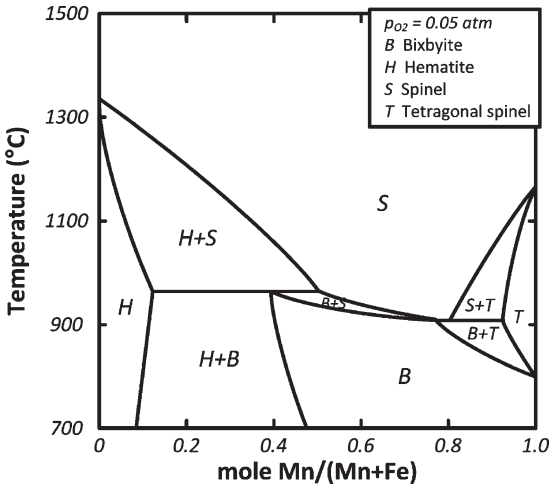

Figure 1. Binary phase diagram of $(Mn_zFe_{1-z})_yO_x$ in an atmosphere with an O_2 partial pressure of 0.05 atm.

experience faster kinetics for O_2 release, and are also capable to operate at higher temperature than unmodified Mn_2O_3–Mn_3O_4. Notably, many variants of the perovskite structure $CaMnO_{3-\delta}$ have been shown to have excellent properties for chemical-looping applications, see Leion et al.[8] and Rydén et al.[9] O_2 release has also been observed with manganese oxides combined with magnesium, silica and nickel, see Shulman et al.[10,11] Many of these materials could be expected to be susceptible to deactivation by fuel impurities such as sulphur though, and thus, may be less useful for applications involving coal and oil. But, there is one possibility that stands out, namely combined oxides of manganese and iron, see Rydén et al.,[12] Azimi et al.,[13] and Shulman et al.[10] The binary phase diagram of combined iron manganese oxide has been examined by Muan and Sōmiya,[14] Wickham,[15] and Crum et al.[16]. In this work a binary phase diagram of the $(Mn_zFe_{1-z})_yO_x$ system has been calculated with the software FactSage using the FToxid database which is shown in Figure 1. Results obtained with FactSage for this system agrees very well with literature data, for example.[17] Thus, the phase diagram gives an accurate representation of the system behavior, although available thermodynamic data for combined oxides of iron and manganese are not precise in detail, see Crum et al.[16]

Figure 1 shows that the fully oxidized states, that is, hematite and bixbyite $(Mn_zFe_{1-z})_2O_3$ are favored at low temperature, while at higher temperature reduced phases like spinel phase $(Mn_zFe_{1-z})_3O_4$ and the tetragonal spinel, hausmannite (Mn_3O_4), are favored. At intermediate temperatures there is a two-phase area in which both oxidized and reduced forms coexist. The reaction of interest for CLOU is decomposition of bixbyite to spinel, see reaction (1), which needs to happen spontaneously in the fuel reactor. Released O_2 would then be instantly consumed by the fuel, facilitating further O_2 release. In the air reactor, reaction (1) is reversed, that is, bixbyite is recreated by oxidation with oxygen from air. The amount of O_2 that can be released by reaction (1) is ≈3.4 wt %.

$$3(Mn,Fe)_2O_3 \leftrightarrow 2(Mn,Fe)_3O_4 + {}^1/_2O_2(g) \qquad (1)$$

Figure 1, also shows that if the surroundings have an O_2 partial pressure of 0.05 atm, reaction (1) goes to the right at temperatures over ≈1340°C for Fe_2O_3, arguably too high to be practicably applicable. The corresponding temperature for Mn_2O_3 is ≈790°C, which according to our experience is too low to obtain reasonably fast reaction kinetics. For mixtures of the two, O_2 release happens at intermediate temperatures. The height of the two-phase area in Figure 1 should correspond roughly to the change in temperature or O_2 partial pressure that will be required to force reaction (1) into completion. Hence Figure 1 suggests that oxide mixtures with Mn/(Mn+Fe) of 0.50–0.80 would be particularly attractive for CLC with oxygen uncoupling. Based on the phase diagram a combined iron manganese oxide with 80% of manganese content could be expected to have very favourable properties, and was therefore selected for examination. The $(Mn_{0.8},Fe_{0.2})_xO_y$ has a very narrow region of two-phase area which means that only a small change in temperature or partial pressure of oxygen can result in a phase shift between reduced and oxidized phase.

Figure 2 shows equilibrium O_2 partial pressure as a function of temperature over $(Mn_{0.8},Fe_{0.2})_xO_y$, calculated with FactSage and FToxid. In a real facility for CLOU, the O_2 concentration in the outlet of the air reactor would need to be low. Else a high degree of excess air will be required, which would reduce the efficiency of the plant. An O_2 partial pressure from the air reactor of 0.05 atm seems reasonable. Figure 2 shows that the combined spinel $(Mn_{0.8},Fe_{0.2})_3O_4$ can be completely oxidized to bixbyite $(Mn_{0.8},Fe_{0.2})_2O_3$ by O_2 partial pressure of 0.05 atm at temperatures below ≈890°C. This is in agreement with previous experiments by Azimi et al.[13] which indicated that $(Mn_{0.8},Fe_{0.2})_xO_y$ was not capable to release oxygen or converting CH_4 in cycles performed at 900 or 950°C. In this work, a temperature of 850°C is selected to be capable of oxidizing $(Mn_{0.8},Fe_{0.2})_xO_y$ completely. In the fuel reactor, released O_2 will be consumed by the fuel. If there is excess oxygen carrier available, O_2 will be released until equilibrium is reached.

There are no thermodynamic restrictions concerning temperature for the fuel reactor. Here, a higher temperature can be used, and is also achievable because the reactions in the fuel reactor are exothermic. A higher temperature here will

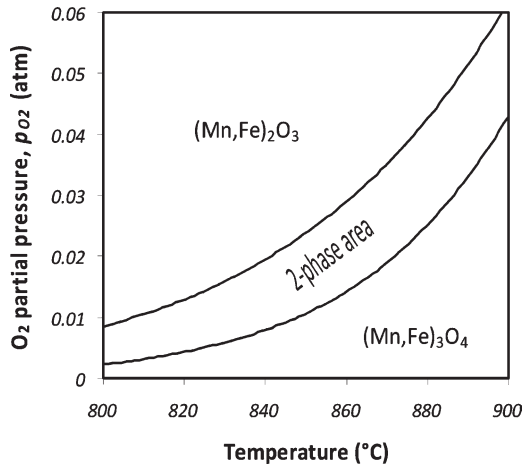

Figure 2. Equilibrium partial pressure of O_2 as function of temperature over $(Mn_{0.8},Fe_{0.2})_xO_y$.

The two phase area constitutes of bixbyite and tetragonal spinel.

Table 1. Physical Properties of Particle

$\overline{d}_p$ (μm)	ρ_{bulk} (kg/m^3)	$\rho_{effective}$ (kg/m^3)	Crushing Strength (N)	BET Surface* (m^2/g)	$\overline{d}_{pore}$ (μm)†	u_{mf} (m/s)‡	u_{mf} (m/s)§
152.5	1043	1800	0.56	2.6	0.45	0.008	0.01

*Measured by Micrometrics Tristar.
†Measured by mercury porosimeter, Micromeritics AutoPore IV.
‡5% oxygen (Air, Nitrogen), 850°C.
§CH_4, 850°C.

increase the equilibrium O_2 partial pressure and likely also be beneficial for the overall reaction kinetics.

Experimental

Material and experimental procedure

Oxygen carrier particles with the composition $(Mn_{0.8},Fe_{0.2})_xO_y$ were produced from powder mixtures of α-Mn_3O_4 and α-Fe_2O_3 by spray drying, according to a procedure described earlier by Azimi et al.[13] The resulting particles were calcined at 950°C for 4 h and sieved to a size range of 125–180 μm. The properties of the fresh material are shown in Table 1. The bulk density of the fresh particles sized 125–180 μm was determined by measuring the mass and volume of a sample of material. A void factor of 0.42 was assumed when calculating the effective density, because this is a theoretical voidage of a normal packed bed with uniformly sized round sand particles with sphericity of 0.86.[18] The crushing strength was measured using a Shimpo FGN-5 device. The presented value is an average of 30 fractured particles sized 180–250 μm. The minimum fluidization velocity (u_{mf}) is calculated based on the relations by Kunii and Levenspiel.[18] The actual superficial velocity in the reactor system is approximately 0.18 m/s for the air reactor and 0.07 m/s for the fuel reactor with CH_4 as fuel. The crystalline phase composition of the fresh oxygen carrier samples was examined with X-ray powder diffraction by a Siemens D5000 powder diffractometer using Cu Kα radiation. The identified phase was bixbyite structure of $(Mn,Fe)_2O_3$.The same phase was detected after testing, that is, after oxidizing period. The O_2 uncoupling properties of the particles were examined by spontaneous decomposition in N_2, as well as by direct reduction with CH_4, and also by reduction with wood char. The experiments were conducted in a quartz reactor with a length of 820 mm and diameter of 22 mm, with a porous quartz plate placed 370 mm from the bottom.

For the N_2 and CH_4 experiments, a sample of 15 g particles was placed onto the quartz plate. The reactor was then heated in an electric furnace, during which the sample was fluidized with 900 mL_n/min (normalized to 1 bar and 0°C) of a gas mixture consisting of 5% O_2 and 95% N_2. When a bed temperature of 850°C was reached, the flow was switched to 600 mL_n/min inert N_2, in order to examine the O_2 uncoupling characteristics of the particles. The flow was then switched back to the O_2/N_2 mixture, and the particles were reoxidized. In this fashion, the sample was exposed to consecutive cycles of oxidizing and inert periods at 850°C. N_2 was used for the O_2 uncoupling experiments, because it is inert, which makes it possible to study the O_2 uncoupling behavior without unwanted interferences. For further reactivity evaluation, the particles were exposed to 365 mL_n/min CH_4, followed by oxidation with the O_2/N_2 mixture. In between each reduction and oxidation, the reactor was purged from reactive gases and gaseous products by introduction of N_2. The particles were tested for 4 days according to the experimental plan shown in Table 2.

For solid fuel experiments, a sample of 10 or 20 g oxygen carrier particles with a size of 125–180 μm was placed onto the porous plate and heated to the temperature of interest in a flow of 1000 mL_n/min of a gas mixture consisting of 5% O_2 and 95% N_2. The particles were then alternatingly exposed to this O_2/N_2 mixture, and reducing periods in which different amounts of wood char, 0.1, 0.4, 0.6, and 1.0 g, were introduced to the bed of oxygen carrier particles. During reducing periods the reactor was fluidized with 900 mL_n/min of pure N_2. Further, 280 mL_n/min of inert sweep gas, that is, N_2, was also introduced to the system at the top of the reactor together with the solid fuel throughout the reducing period to ensure that the pulverized fuel did not get stuck in the feed line. This sweep gas did not enter the hot reaction zone of the reactor. The oxidation and the reduction periods were separated by an inert period with 900 mL_n/min of pure N_2 for 60 s. In order to verify reproducibility, all solid fuel experiments were carried out three times each.

The solid fuel used for these tests was a Swedish wood char with 11% volatiles, 3% moisture, and 3% ash.

The gas from the reactor was led to an electric cooler for removing water and then to a Rosemount NGA 2000 Multi-Component gas analyzer, measuring the concentrations of CO, CO_2, and CH_4 with measurement at infrared spectral range, O_2 with paramagnetic oxygen measurement (PO_2) and also the gas flow. Gases were analyzed with a frequency of 0.5 Hz and uncertainty of around 2% on the measured value. All flows are given at normal conditions, that is, 0°C and 1.013 bar. The temperature was measured 5 mm under and 10 mm above the porous quartz plate using Pentronic CrAl/NiAl thermocouples with inconel-600 enclosed in quartz shells. The temperature presented in the article is the set-

Table 2. Experimental Plan

Day	No. of Cycles	Red. Gas	F_{Ox} (L_n/min)	F_{In} (L_n/min)	t_{In} (s)	F_{Red} (L_n/min)	t_{Red} (s)	T (°C)
1	4	N_2	0.9	0.6	360	–	–	850
	4	CH_4	0.9	0.6	60	365	20	850
2	3	N_2	0.9	0.6	360	–	–	850
	2	CH_4	0.9	0.6	60	365	20	850
	1	CH_4	0.9	0.6	60	365	40	850
3	5	CH_4	0.9	0.6	60	365	20	850
4	1	CH_4	0.9	0.6	60	365	40	850

F_x is flow during Ox(idation), Red(uction), and In(ert)

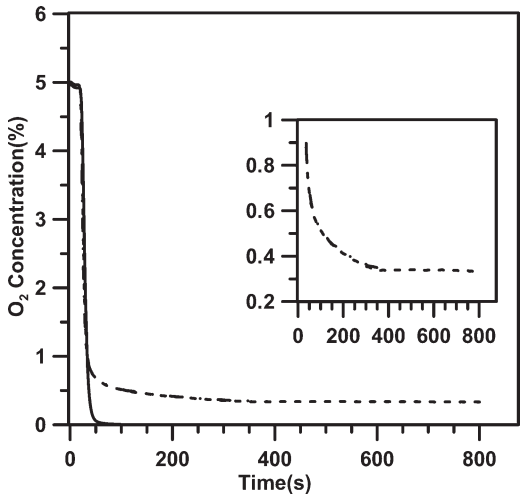

Figure 3. Oxygen concentration vs. time during inert period at 850°C, dashed lines.

Solid line shows response in absence of oxygen carrier (in sand).

point temperature, that is, the temperature at the beginning of the reduction. From high frequency measurements of the pressure drop, it was possible to see if the bed was fluidized.

The oxygen release of the iron-manganese oxide was also investigated using a thermogravimetric analyzer (NETZSCH model STA 409 PC Luxx). The experiment was performed in an inert N_2 atmosphere using a simple temperature profile that heats the sample at a rate of 20°C/min to 1250°C. The particles were kept at the temperature of 1250°C for 30 min after which the sample is cooled at 20°C/min to 200°C. The amount of oxygen released from the sample can be judged by the measured mass change as a function of temperature.

Data evaluation

The degree of conversion, X, defines the extent to which the oxygen carriers are oxidized and is defined as follow:

$$X = \frac{m - m_{\text{red}}}{m_{\text{ox}} - m_{\text{red}}} \tag{2}$$

where m is the actual mass of the sample, m_{ox} is the mass of the fully oxidized sample, and m_{red} is the mass of the sample in its fully reduced form. Here, the fully oxidized form is $(Mn_zFe_{1-z})_2O_3$ and fully reduced form is $(Mn_zFe_{1-z})_3O_4$.

The degree of conversion of oxygen carrier during reduction with methane as a function of time is calculated from the outlet gas concentrations using Eq. 3.

$$X_i = X_{i-1} - \int_{t_0}^{t_1} \frac{1}{M_0 P_{\text{tot}}} \dot{n_{\text{out}}} (4p_{CO_2,\text{out}} + 3p_{CO,\text{out}} + 2p_{O_2,\text{out}} - p_{H_2,\text{out}}) dt \tag{3}$$

Similarly, the degree of conversion for N_2 period can be calculated using Eq. 4.

$$X_i = X_{i-1} - \int_{t_0}^{t_1} \frac{1}{M_0 P_{\text{tot}}} (\dot{n_{\text{out}}} p_{O_2,\text{out}}) dt \tag{4}$$

Moreover, the degree of conversion during reduction with wood char is described by means of Eq. 5.

$$X_i = X_{i-1} - \int_{t_0}^{t_1} \frac{1}{M_0 P_{\text{tot}}} \dot{n_{\text{out}}} (p_{\text{CO}_2,\text{out}} + 0.5p_{\text{CO,out}} + p_{\text{O}_2,\text{out}} - (O_2/C)_{\text{fuel}} p_{\text{c,tot}} + (0.5(\text{H}_2/\text{C})_{\text{fuel}} p_{c,\text{tot}} - 0.5p_{H_2,\text{out}} - p_{\text{CH}_4,\text{out}})) dt \tag{5}$$

where X_i is the conversion as a function of time for a period i, X_i-1 is the degree of conversion after the former period; t_0 and t_1 are respectively the times for the start and the finish of the period; M_0 is the moles of active oxygen in the unreacted oxygen carrier; n_{in} and n_{out} are the molar flows of dry gas entering and exiting the reactor, respectively; P_{tot} is the total pressure; $p_{\text{CO}_2,\text{out}}$, $p_{\text{H}_2\text{out}}$, $p_{\text{CO,out}}$, and $p_{\text{CH}_4,\text{out}}$ are the outlet partial pressures of CO_2, H_2, CO, and CH_4 after removal of water vapour, respectively and $p_{\text{O}_2,\text{out}}$ is the partial pressure of exiting oxygen; $(O_2/C)_{\text{fuel}}$, $(H_2/C)_{\text{fuel}}$ are the estimated molar ratios of oxygen and hydrogen over carbon in the fuel; and $p_{\text{c,tot}}$ is the total partial pressure of carbon, that is, $p_{\text{CO2,out}} + p_{\text{CO,out}} + p_{\text{CH}_4,\text{out}}$.

The oxygen ratio of oxygen carrier, R_0, is defined as below:

$$R_0 = \frac{m_{\text{ox}} - m_{\text{red}}}{m_{\text{ox}}} = \frac{m_0}{m_{\text{ox}}} \tag{6}$$

where m_0 is the mass of active oxygen in the unreacted oxygen carrier. The R_0 value for $(Mn_{0.8},Fe_{0.2})_2O_3$ is equal to 0.0337.

For analysis of the gas fuel conversion, the fraction of methane being fully oxidized to CO_2 in the outlet gas flow was calculated on dry basis as follows:

$$\gamma = \frac{p_{\text{CO}_2}}{p_{\text{CH}_4} + p_{\text{CO}_2} + p_{\text{CO}}} \tag{7}$$

Results and Discussion

In the first series of experiments, which involved decomposition of oxygen carrier in nitrogen, called inert period, the sample initially released O_2 so that an O_2 concentration of ≈0.8–0.9% was achieved. The O_2 concentration then slowly decreased as a function of time until it reached ≈0.35%, where it stabilized. Figure 3 shows the results for one such inert period lasting 360 s, and also one extra longer period of 800 s to check the stability of the oxygen equilibrium level. The concentration is below the lower boundary of the two-phase area in Figure 2, but as was explained above, the thermodynamic data for these combined oxides are not very precise. Moreover, the particles are releasing oxygen in a stream of nitrogen and depending on the kinetics of the oxygen release, the concentration should be lower than the thermodynamic equilibrium.

Additional experiments conducted in a thermogravimetric analyzer show that it was possible to release all available oxygen, that is, ≈3.4 wt %, without influence of fuel.

Figure 4 demonstrates the outlet dry gas concentration for reduction with CH_4.

In Figure 4, the air is shifted to nitrogen at the time 20 s. The figure shows that the iron manganese oxide spontaneously decomposes giving ≈0.6% of oxygen in the exiting gas. At the time 80 s gaseous fuel, methane, is added for 40 s. Methane reacts directly with the oxygen released from the $(Mn_{0.8},Fe_{0.2})_xO_y$ producing CO_2 and heat, which results in a temperature increase promoting the spontaneous release of

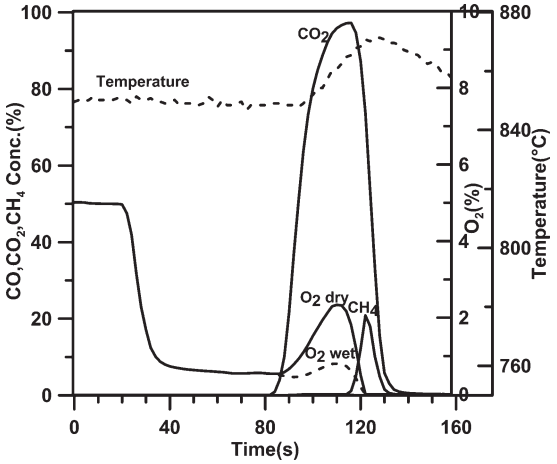

Figure 4. Measured dry gas concentrations during 40 s reduction of 15 g $(Mn_{0.8},Fe_{0.2})_xO_y$ with 365 mL_n/min CH_4 at 850°C

O_2. The O_2 uncoupling was sufficiently fast for producing a concentration of CO_2 close to 100%. Before fuel is added, the oxygen concentration is 0.5–0.6%, corresponding to an oxygen flow of 5 mL_n/min. The oxygen in the CO_2 comes from the oxygen carrier, so when fuel is added oxygen is released from the particles at a rate which is able to oxidize a methane flow of 365 mL_n/min, which means an oxygen flow of 730 mL_n/min from the particles. Thus, the oxygen release is increased by two orders of magnitude. At the same time, the measured oxygen concentration, that is, measured on dry basis is increased by roughly a factor of three, see Figure 4. This is mainly an artifact caused by the steam produced in the reaction with methane, giving two H_2O per CO_2 in the outlet gas. Figure 4 also shows the calculated O_2 concentration on wet basis, that is, the actual concentration at the outlet of the reactor, and as seen this is reasonably constant. This would also be expected if the oxygen concentration is mainly controlled by the thermodynamic equilibrium. This suggests a very rapid O_2 release, considering the large quantities of oxygen consumed by the fuel. Another factor influencing the results is that the reaction between CH_4 and $(Mn_{0.8},Fe_{0.2})_2O_3$ is exothermic. Hence, the temperature in the sample bed increases ≈20 K during experiments with CH_4, which according to Figure 2 should increase the equilibrium partial pressure of O_2 over the sample somewhat.

The complete conversion of methane to CO_2 continues until almost all $(Mn,Fe)_2O_3$ is spent, This is shown in Figure 5, depicting the gas fuel conversion (γ), for the same test, as a function of the oxygen carrier conversion (X). Here, $X = 0$ means that all $(Mn,Fe)_2O_3$ has been converted to $(Mn,Fe)_3O_4$. Thus, the methane peak in the end of the period is a result of a depletion of the $(Mn,Fe)_2O_3$ in the particles. Thus, reaction (1) can proceed until ≈3.4 wt % O_2 has been released from the sample. After this point, $(Mn,Fe)_3O_4$ can be further reduced to MnO and FeO by gaseous fuel. This further reduction cannot release O_2 in gas phase though, and is not capable of providing complete conversion of CH_4.

There is some backmixing of the gas before it reaches the analyzer. As seen in Figure 4, the initial slope in O_2 concentration when nitrogen is turned on is ~10 s long. The same effect is seen during the reducing period for CO_2, CO, and CH_4. Similar transients of approximately 10 s due to back mixing are expected when oxygen release from the particles is slowing down and methane starts to appear in the outlet gas. This would explain the overlapping period in Figure 4 when O_2 and CH_4 are measured simultaneously during 10 s. The actual concentration of O_2 in the reactor likely goes to zero as methane starts to rise rapidly.

Figure 5 shows that the conversion of the material, X, is around 85% when gas conversion starts to drop, that is, when CH_4 starts to appear in Figure 4. Here, it should be pointed out that this result is also affected by the backmixing of the gas. As a consequence of backmixing, the drop in conversion shown in Figure 5 becomes smoother, whereas the real drop in conversion shows up at a higher value of X, more likely around 0.95, and is much steeper.

The $(Mn_{0.8},Fe_{0.2})_xO_y$ particles were examined in multiple reduction and oxidation periods for 4 days, see Table 2. The results were consistent and very encouraging, and no fluidization problem or other operational problems were encountered during the experiments. Figures 4–5 shows that the particles were able to release essentially all of its oxygen in 40 s. The data suggests that the main mechanism is through oxygen uncoupling and not direct reaction of oxygen carrier and methane. However, to obtain conclusive evidence for the oxygen uncoupling mechanism, further tests were performed with wood char, where the possibility of direct solid–solid reaction in the fluidized bed is essentially eliminated.

Data for one of the solid fuel tests are shown in Figure 6. Here, the corrected outlet gas concentrations, that is, gas concentration disregarding dilution by the sweep gas, are shown as a function of time for reduction of 10 g $(Mn_{0.8},Fe_{0.2})_2O_3$ particles with 0.6 g wood char at 850°C. The oxygen concentration during oxidation is 5%. When the fluidizing gas is switched to nitrogen, the oxygen concentration decreases to around ≈0.5%, analogous with Figures 3–4. When the fuel is introduced to the reactor, peaks of CH_4 and CO can be seen in the beginning of the reaction due to devolatilization of the fuel. Simultaneously, the CO_2 concentration increases since the combustion of volatiles and char starts instantly. By inserting the solid fuel into the reactor, the oxygen concentration falls to zero as the fuel consumes all released oxygen. The zero concentration of oxygen and high concentration of CO_2 shows that the decomposition

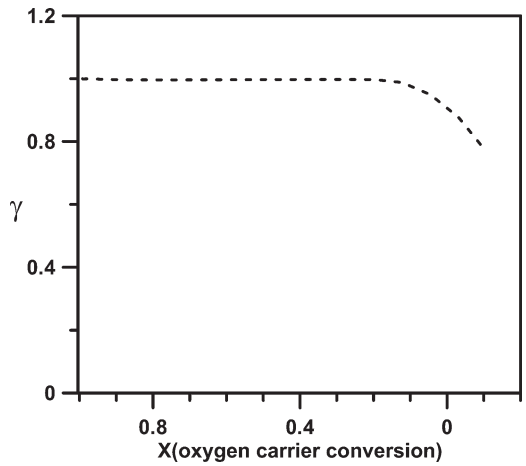

Figure 5. Gas fuel conversion (γ) against the oxygen carrier conversion (X) for reduction with methane.

reaction of $(Mn,Fe)_2O_3$–$(Mn,Fe)_3O_4$ is occurring without any thermodynamic barrier. When the rapid initial devolatilization is finished, the remaining char can only be converted by reaction with oxygen released from the oxygen carrier. This is because the fluidizing gas is nitrogen, so there is no gasification. Thus, evolved CO_2 is a measure of oxygen release.

The results for fuel tests using lower ratios of fuel to oxygen carrier particles showed similar behaviour, with the exception of lower CO_2 concentration and also higher O_2 level. The oxygen level for these experiments does not fall to zero and also increases with the increasing temperature due to the exothermic reaction of the fuel combustion. The excess of oxygen in these experiments shows that the amount of fuel for these cases was insufficient to remove all evolved oxygen, indicating that the fuel combustion is limiting the overall reaction. Figure 7 shows the oxygen carrier conversion as a function of time for both a CH_4 cycle and the solid fuel cycles. In Figure 7, time starts when fuel is added, and because of oxygen release during the preceding inert period, X is slightly less than 1. The denotation of $\frac{\text{Fuel}(g)}{\text{O.C.}(g)}$ in Figure 7, is used to indicate the ratio of the mass of wood char to oxygen carrier.

Figure 7 demonstrates that by increasing the mass ratio of fuel to oxygen carrier, the rate of oxygen carrier conversion also increases. It also shows that for full reduction of oxygen carrier ($X = 0$), sufficient amounts of fuel is needed. The test with the highest char to oxygen carrier ratio, $\frac{\text{Fuel}(g)}{\text{O.C.}(g)} = \frac{0.6}{10}$, is the case where the maximum oxygen removal rate from the oxygen carrier was achieved. Here, the oxygen carrier is almost fully reduced and the rate of oxygen carrier conversion is similar to the test with CH_4. This was also the only solid fuel test where the oxygen concentration reached zero. Two different cycles of $\frac{\text{Fuel}(g)}{\text{O.C.}(g)} = \frac{0.6}{10}$ (C.1 and C.2) are presented in Figure 7. As seen, the initial slope, during first 30 s, is similar but there is a deviation in the final conversion. This is likely a result of errors in the mass balance caused by uncertainties in the calculation of the gas flow.

Figure 7 shows that for the tests with $\frac{\text{Fuel}(g)}{\text{O.C.}(g)} = \frac{0.6}{10}$ and CH_4, the oxygen carrier becomes fully reduced in around 40 s. Considering concentration transients caused by the backmixing, the conversion time seen in Figure 7 is overestimated

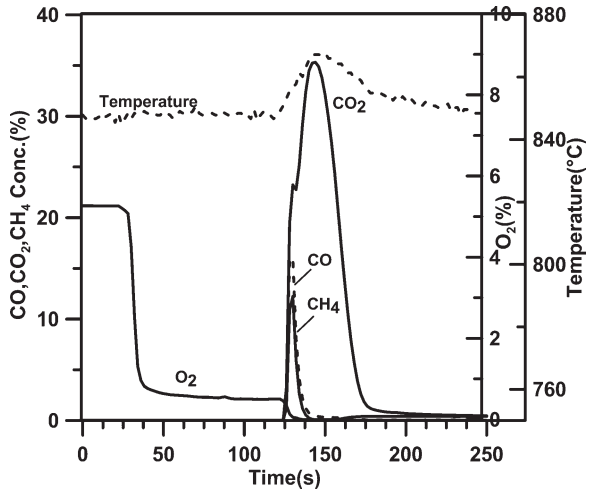

Figure 6. Measured dry gas concentrations during the reduction of 10 g $(Mn_{0.8},Fe_{0.2})_2O_3$ with 0.6 g Swedish wood char at 850°C

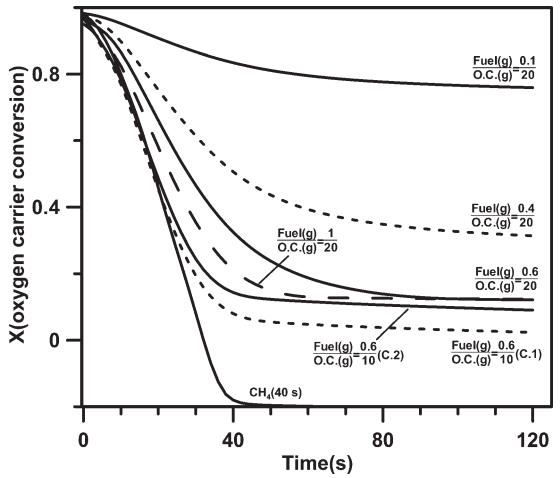

Figure 7. Oxygen carrier conversion, (*X*), vs. time for both CH_4 cycle and solid fuel cycles.

by around 10 s. Thus, most of the oxygen is released in about 30 s. The rapid release of oxygen in the solid fuel experiments, supports the presumption that the main reaction mechanism between methane and $(Mn_{0.8},Fe_{0.2})_xO_y$ is by oxygen release in gas phase.

As for Figure 7, the minimum limit of X for solid fuel test is 0, in contrast with the gas fuel test in which X can be reduced below 0 due to further reduction to MnO–FeO.

Difficulties were noted for oxidizing the oxygen carrier particles following reduction in some of the experiments, both with gaseous and solid fuel. For gaseous fuel experiments with 40 s reduction time, in which the particles were fully reduced, there was some delay in oxidation of $(Mn,Fe)_3O_4$–$(Mn,Fe)_2O_3$. The observed induction time during reoxidation of particles was correlated to cases with full reduction of material. This induction time has also been observed by Lambert et al.[19] This delay is likely attributed to the fact that there is no $(Mn,Fe)_2O_3$ to start with, that is, a temporary deviation from thermodynamics corresponding to the case of for instance a super cooled liquid. For solid fuel experiments, by adding more fuels, the oxidation became slower. Therefore, in the solid fuel tests with the highest oxygen carrier reduction, $\frac{\text{Fuel}(g)}{\text{O.C.}(g)} = \frac{0.6}{10}$, difficulties with starting the oxidation was solved by reducing the oxidation temperature to 800°C. This is also in accordance with thermodynamics, as a temperature decrease facilitates oxidation by lowering the equilibrium partial pressure, Figure 2. But, oxidation in all other tests was at normal temperature. It can be added that it is highly unlikely that a real process would be operated in such a way that particles would be fully reduced.

To illustrate the implications of the rates measured an example is given here. If it is assumed that the oxygen carrier transfers oxygen corresponding to 2% of its mass in each cycle, this would correspond to a solids circulation between air and fuel reactor of 230 kg/min,MW. The presented rates suggest that a residence time of less than 30 s could be sufficient for the release of oxygen in presence of fuel. This would then, with the given circulation rate corresponds to a solids inventory of only 115 kg/MW for the fuel reactor.

Conclusions

The study indicates that $(Mn_{0.8},Fe_{0.2})_xO_y$ can be used as oxygen carrier material for CLC with oxygen uncoupling (CLOU). The results show rapid oxygen release and complete

conversion of CH_4 into CO_2 and H_2O at 850°C. The rapid release of oxygen was also verified by using wood char as fuel, where any solid–solid reaction between char and oxide particles would be negligible. It is shown that $(Mn_{0.8},Fe_{0.2})_xO_y$ is able to release gas phase oxygen corresponding to around 3.4% of its mass. Moreover, most of this oxygen can be released in only 30–40 s in presence of a fuel. Such a large and rapid oxygen release has previously only been seen with the CuO–Cu_2O system. This finding suggests that it would be possible to manufacture highly reactive oxygen carrier particles suitable for oxidation of solid fuels from very cheap and environmentally benign raw materials, and could be of great importance for further development of chemical looping combustion technologies.

Acknowledgments

This publication was based on work supported by the Swedish Energy Agency project number 32368-1.

Literature Cited

1. Lyngfelt A, Mattisson T. *Materials for chemical-looping combustion*. In: D. Stolten and V. Sherer, editors. *Efficient Carbon Capture for Coal Power Plants*, editors. Weinheim: Wiley-VCH Verlag GmbH & Co. KGaA, 2011.
2. Lyngfelt A. Oxygen carriers for chemical-looping combustion – 4000 h of operational experience. *Oil Gas Sci Technol*. 2011;66: 161–172.
3. Fang H, Haibin L, Zengli Z. Advancements in development of chemical-looping combustion: a review. *Intl J of Chem Eng*. 2009; doi:10.1155/2009/710515.
4. Hossain M, De Lasa H. Chemical looping combustion (CLC) for inherent CO2 separations-a review. *Chem Eng Sci*. 2008;63:4433–4451.
5. Mattisson T, Leion H, Lyngfelt A. Chemical-looping with oxygen uncoupling using CuO/ZrO2 with petroleum coke. *Fuel*. 2009;88:683–690.
6. Leion H, Mattisson T, Lyngfelt A. Using chemical-looping with oxygen uncoupling (CLOU) for combustion six different of solid fuels. *Energy Procedia*. 2009;1:447–453.
7. Mattisson T, Lyngfelt A, Leion H. Chemical-looping with oxygen uncoupling for combustion of solid fuels. *Intl J Greenhouse Gas Control*. 2009;3:11–19.
8. Leion A, Larring Y, Bakken E, Bredesen R. Use of CaMn0.875-Ti0.125O3 as oxygen carrier in chemical-looping with oxygen uncoupling. *Energy Fuels*. 2009;23:5276–5283.
9. Rydén M, Lyngfelt A, Mattisson T. CaMn0.875Ti0.125O3 as oxygen carrier for chemical-looping combustion with oxygen uncoupling (CLOU)–experiments in a continuously operating fluidized bed reactor system. *Intl J Greenhouse Gas Control*. 2011;5:356–366.
10. Shulman A, Cleverstam E, Mattisson T, Lyngfelt A. Manganese/iron, manganese/nickel, and manganese/silicon oxides used in chemical-looping with oxygen uncoupling (CLOU) for combustion of methane. *Energy Fuels*. 2009;23:5269–5275.
11. Shulman A, Cleverstam E, Mattisson T, Lyngfelt A. Chemical – looping with oxygen uncoupling using Mn/Mg-based oxygen carriers – oxygen release and reactivity with methane. *Fuel*. 2011;90: 941–950.
12. Rydén M, Lyngfelt A, Mattisson T. Combined manganese/iron oxides as oxygen carrier for chemical looping combustion with oxygen uncoupling (CLOU) in a circulating fluidized bed reactor system. *Energy Procedia*. 2011;4:341–348.
13. Azimi G, Leion H, Mattisson T, Lyngfelt A. Chemical-looping with oxygen uncoupling using combined Mn-Fe oxides, testing in batch fluidized bed. *Energy Procedia*. 2011;4:370–377.
14. Muan A, Sōmiya S. The system of iron oxide-manganese oxide in air. *Am J Sci*. 1962;260:230–240.
15. Wickham D. The chemical composition of spinels in the system Fe3O4-Mn3O4. *J Inorg Nuclear Chem*. 1969;31:313–320.
16. Crum JV, Riley BJ, Vienna JD. Binary phase diagram of the manganese oxide – iron oxide system. *J Am Ceram Soc*. 2009;92: 2378–2384.
17. Kjellqvist L, Selleby M. Thermodynamic Assessment of the Fe-Mn-O System. *J Phase Equilib Diffus*. 2010;31:113–134.
18. Kunii D, Levenspiel O. *Fluidization Engineering*. Stoneham: Reed publishing Inc., 1991.
19. Lambert A, Delquié C, Clémeneçon I, Comtea E, Lefebvrea V, Rousseau J, Durand B. Synthesis and characterization of bimetallic Fe/Mn oxides for chemical looping combustion. *Energy Procedia*. 2009;1:375–381.

Manuscript received Jan. 31, 2012, and revision received Apr. 18, 2012.